SELECTED TOPICS TOWARD THE EXPERIMENTAL DESIGN OF A WAVEGUIDE CONFINED RAMAN LASER WAVELENGTH CONVERSION SYSTEM

by

Michael Ryan Hintzman

A professional paper submitted in partial fulfillment
of the requirements for the degree

of

Master of Science

in

Electrical Engineering

MONTANA STATE UNIVERSITY
Bozeman, Montana

November 2011

APPROVAL

of a professional paper submitted by

Michael Ryan Hintzman

This professional paper has been read by each member of the thesis committee and has been found to be satisfactory regarding content, English usage, format, citation, bibliographic style, and consistency and is ready for submission to The Graduate School.

Dr. Joseph Shaw

Approved for the Department of Electrical & Computer Engineering

Dr. Robert Maher

Approved for The Graduate School

Dr. Carl A. Fox

STATEMENT OF PERMISSION TO USE

In presenting this thesis in partial fulfillment of the requirements for a master's degree at Montana State University, I agree that the Library shall make it available to borrowers under rules of the Library.

If I have indicated my intention to copyright this professional paper by including a copyright notice page, copying is allowable only for scholarly purposes, consistent with "fair use" as prescribed in the U.S. Copyright Law. Requests for permission for extended quotation from or reproduction of this thesis in whole or in parts may be granted only by the copyright holder.

Michael Ryan Hintzman

November 2011

ACKNOWLEDGMENTS

I would like to acknowledge my advisor, Dr. Joseph Shaw, who guided me in my classes, and my project advisor, Dr. Zeb Barber, who allowed me to work on the project and assisted me with understanding the project goals. I would also like to acknowledge Dr. Randy Reibel for guiding me and helping me with growing my laboratory skill set. I would finally like to acknowledge Christoffer Renner, who has been a valuable source of knowledge with experimental setups and techniques that greatly helped me.

TABLE OF CONTENTS

TABLE OF CONTENTS - CONTINUED

LIST OF TABLES

Table Page

LIST OF FIGURES

Figure Page

ABSTRACT

As an alternative to current visible variable-wavelength lasers, a Raman conversion laser system was studied using a hollow-core capillary. A pulsed Nd:YAG laser is frequency doubled to 532 nm using a KTP crystal prior to coupling into the capillary that is pressurized from 0 PSI to 100 PSI with either CO_2 or H_2 gas. The KTP crystal is then removed and found that the 1064 nm laser light is phase-matched when coupled into the capillary. The phase-matched coupled light produces observable third anti-Stokes light, while suppressing the higher Stokes conversion light. The methods used to couple a laser beam into a hollow-core glass capillary, examination of the acceptance angle of a KTP crystal, and the Raman conversion wavelengths due to 1064 nm laser pulses are documented in this paper.

CHAPTER 1 – INTRODUCTION

Problem and Motivation

A need recently arose at the Montana State University (MSU) Spectrum Lab for a laser system that is capable of producing high-energy laser pulses, with a top hat temporal pulse profile, at adjustable visible wavelengths. The emphasis is on the need for high-energy laser pulses with a variable visible wavelength. The United States Navy has asked for solutions to this problem to be used for on-board ship defense against incoming missiles and reconnaissance drones. The idea is that the laser pulses will disrupt and/or destroy the imaging sensor that the missile uses for targeting, or that the laser pulses will blind the imaging sensor used by the drone for reconnaissance. In order to prevent the image sensor from easily negating the laser pulse by inserting a band-rejection filter, the Navy has also requested that the laser system be able to generate a variety of wavelengths in the visible spectrum. The Navy requested a laser to be developed that produces a visible laser pulse outside of the 510 nm to 550 nm wavelength band, with power in excess of 50 mJ per pulse, a pulse duration in the range of 100 to 200 ns, and with excellent spatial beam quality ($M^2<2$) [1].

To achieve the high power and variable wavelength goals, several different laser systems could have been considered before the Raman scattering system was selected by MSU-Spectrum Lab. These laser systems include dye lasers, second harmonic generation of a tunable near infrared laser, free electron lasers, and an optical parametric oscillator (OPO) laser based on the 3rd harmonic of the common 1064 nm Nd:YAG laser. The dye

laser is not an attractive option because the laser medium is a known carcinogen, causing extra hazards that would need to be accounted for. Another drawback of the dye laser is that the system is bulky and messy, as the dye must be poured into a reservoir in the laser system.

The use of a tunable near infrared laser that is frequency doubled could also be considered as a potential laser system. However, these systems are less desirable because of the limited number of visible wavelengths that it is capable of obtaining. There have been tunable laser systems developed using this technique capable of a wavelength range from 300 nm to 970 nm; however, these systems have low energy per pulse, for example, 870 nJ at 14 fs pulse duration [2].

Another solution to the problem pursued by the Navy is the free electron laser. This type of laser is capable of producing the desired energy levels at a wide range of wavelengths. The laser requires a large area to propel the electrons such that photons are produced at the designed wavelength. This results in excessive physical size and complexity, which makes it totally inappropriate for this application. Recent developments have decreased the physical size of free-electron lasers, the other laser system choices still possess a significantly smaller bench footprint.

An OPO that is pumped with a frequency tripled NIR source could possibly be the best laser system to use for this study. One OPO system is capable of producing 1.2 mJ in the 245 to 260 nm range, 4.8 mJ at 355 nm, and 8.8 mJ at 532 nm at pulse lengths of 4 ns [3]. This system also exceeded the beam quality factor specification with an M^2 value of 1.5. However, Spectrum Lab experience led to the decision to instead pursue a

Raman conversion laser system as a research study into the efficiency that could be achieved with this new approach.

A primary motivation for investigating a laser solution based on Raman conversion is that this approach will allow for the variable visible wavelength selection. It has been shown that this laser system is capable of producing multiple wavelengths (1st and 2nd Stokes conversion and 1st Anti-Stokes conversion) in the Raman medium [4]. The Raman gas will take the stabilized pulse laser output (1064 nm or 532 nm if the beam is frequency doubled) and convert it to a wide wavelength range depending on the pressure of the gas, polarization, and the gas chosen.

The proposed laser system also could have other nonmilitary use in atmospheric studies for light detection and ranging (LIDAR). Using the Raman conversion with specific gases, the laser wavelength is able to reach from the ultraviolet to the mid-wave infrared (~5 microns). This allows for the laser to be used in a LIDAR system that can be operated at eye-safe wavelengths (typically > 1.5 μm) for detecting a wide range of gases in the atmosphere.

Role in Project and Other Proposed Solutions

My role in this project was to assist the program manager and Spectrum Lab personnel with setting up the laboratory bench and running experiments. The experiments consist of: operating and optimizing the laser source, coupling into a Raman conversion waveguide, and separating the generated wavelengths from the source wavelength. Each

experiment provided me with improved skills to conduct the next experiment in the order shown in Figure 1.1.

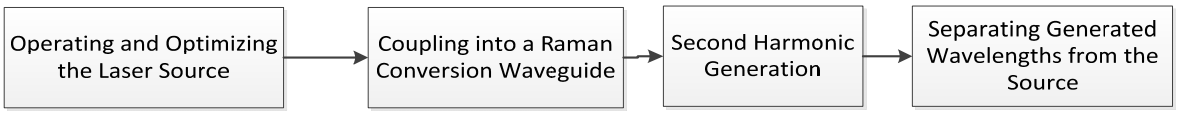

Figure 1.1: Experimental Flow Chart

The experiments were in line with the goals of the Navy contract and consist of me, under the guidance of a more senior researcher, optimizing and operating the 1064 nm laser source, coupling the laser into the capillary such that the propagating mode was the TE_{01} mode for optimal Raman conversion, conducting experiments to understand the acceptance angle of a second harmonic generation crystal, and observing the Raman converted wavelengths using a reflection diffraction grating.

CHAPTER 2 – EXPERIMENTAL SETUP AND LASER DESIGN

Introduction

The laser system utilized is documented in the MSU Physics Master's Thesis by Stephen Scott Wagemann [5]. The laser is designed to produce a pulsed beam of 1064 nm light. A potassium titanyl phosphate (KTP) crystal is used to double the frequency of the light to 532 nm, which allows for Raman conversion in the visible spectrum using hydrogen and carbon dioxide gases as the Raman medium. The beam is then spatially filtered and the polarization is set prior to coupling into the hollow-core capillary. This chapter discusses the lab bench setup of the laser system, as well as the experimental setup for coupling into the hollow-core capillary.

Experimental Setup

The laser is seeded with a diode-pumped solid state laser, with the output passing through a half-wave plate and a polarizer to control the beam power. A beam-splitter cube is placed before an acousto-optic modulator (AOM) that is driven by a waveform generator. The AOM and waveform generator is used to create the desired waveform pulse. An optical isolator is used to prevent reflected light from proceeding into the seed laser and causing unwanted feedback. The laser pulse is then double passed through a pre-amplifier followed by two main amplifiers. An additional optical isolator is placed before each of the main amplifiers to suppress pre-lasing in the main amplifiers. The laser pulse is then directed into the KTP crystal, in which the pulse undergoes Second

Harmonic Generation to produce a wavelength of 532 nm [5]. The laser system layout is shown in Figure 2.1 with Figure 2.2 showing the spatial filtering and coupling portion of the setup.

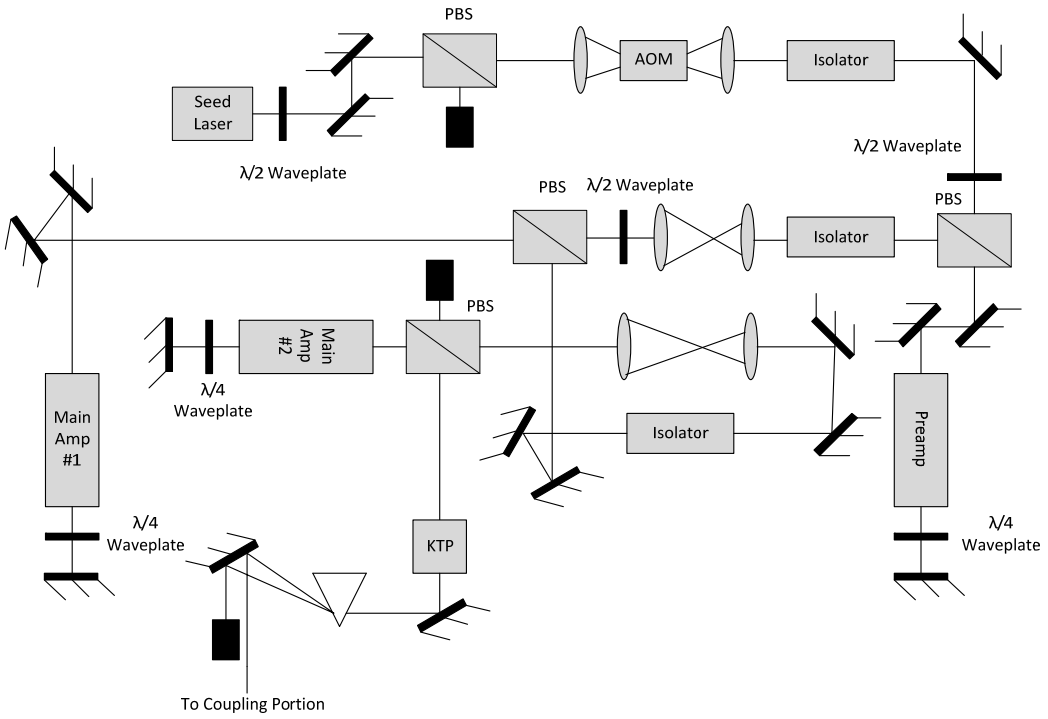

Figure 2.1: Laser Amplification Setup

After second harmonic generation the laser pulse is passed through a prism to separate the pump (1064 nm) wavelength from the Second Harmonic Generation (532 nm) wavelength. The pulse is then passed through two spatial frequency filters to remove energy that is present in the edges of the spatial mode. This is to ensure that the capillary is protected from light that is not able to be coupled into the hollow core. The light pulse, if not properly coupled into the core, can damage the glass cladding. Once the

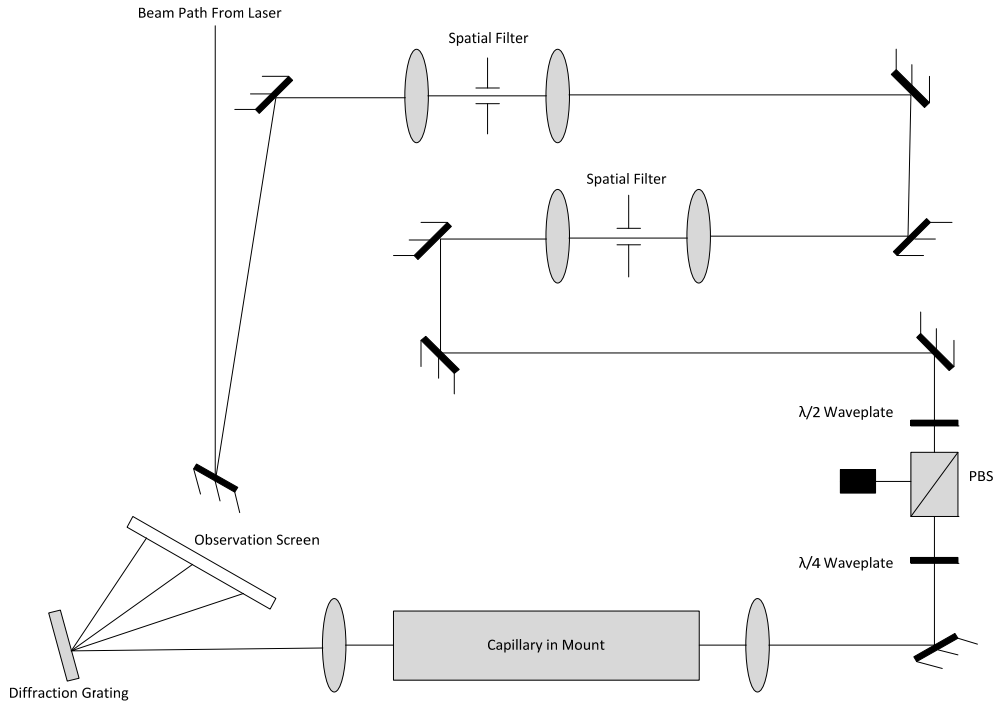

Figure 2.2: Laser Coupling Setup

cladding is damaged, the coupling efficiency drops significantly and conversion in the hollow core capillary goes to zero.

A half-wave plate is used to rotate the polarization of the light that is incident on the polarizing beam splitter (PBS) to provide control of the power of the beam incident on the capillary, and the quarter wave-plate controls the ellipticity of the beam coupling into the capillary. By changing this polarization, the Raman conversion can be changed between the vibrational (linear polarization) and rotational (circular polarization) conversion wavelengths. To ensure that the pulse is properly coupled into the capillary, two cameras are used and the laser is set to CW mode. One camera is used to observe the coupling from the front of the capillary and a second camera is used to monitor the coupling from the back of the capillary. The laser beam is steered using two beam

steering mirrors until a single mode is observed, indicating that the laser beam is being efficiency coupled into the capillary for Raman conversion.

The capillary is mounted in a custom gas cell block that was designed and machined by Spectrum Lab research associate Christopher Renner. The cell block is constructed from aluminum, and consists of a v-block that holds the capillary in space. The capillary is capped with an aluminum block that has a glass window on each end, with one end having a valve to pressurize the capillary. A second gas cell is also utilized. This gas cell pressurizes the capillary itself and the volume around the capillary. This design reduces the strain that the custom gas cell block puts on the glass capillary. The laser pulse is then directed onto a grating, which diffracts the seed wavelength from the Raman converted light. An observation screen with a camera directed on it is used to observe and record the output.

CHAPTER 3 – COUPLING A LASER BEAM INTO A HOLLOW CORE CAPILLARY

Introduction

The ability to control the direction of propagation for a laser beam is a unique ability of waveguides. Most waveguides are optical fibers with solid cores, yet waveguides can also be hollow-core capillaries, which are used in this experiment. As a light wave couples into a waveguide, the light can propagate through the waveguide in a variety of resonance modes determined by the waveguide geometry and optical wavelength. Typically propagation entirely within the fundamental or lowest order mode is desired, as this mode allows for the maximum amount of energy to be propagated through the waveguide. This experiment will focus on how to couple a laser beam into a hollow-core capillary and the energy loss associated with the transmission through the waveguide.

Theory

The ability to couple a laser beam into a waveguide in the desired optical mode is dependent upon a few key parameters. These parameters include the diameter of the waveguide itself, the diameter of the laser beam spot, and the desired propagating mode. In order to determine the optimal size of the beam spot, and thus which focusing optic to use, the optimal beam waist is calculated using the ratio of the beam waist, ω, and the core radius, a. For a minimum loss through the waveguide, the ratio ω/a is desired to be 0.64 as this is the point when the propagating mode of a Gaussian laser beam mode

closely matches with the waveguide [6]. When the laser beam is mode matched with the waveguide, the maximum amount of power is coupled into the waveguide.

Coupling the laser beam into the waveguide such that it is mode matched requires a lens with a focal length chosen to match the Gaussian beam focusing size according to Eq. 3.1 (it also requires a diffraction-limited lens).

$$f = \frac{D_c d}{1.22\lambda} \tag{3.1}$$

To calculate the required coupling lens focal length, the diameter of the waveguide, *d,* is multiplied with the diameter of the collimated laser beam, D_c. This product is divided by 1.22 multiplied by the wavelength of the laser beam, λ.

Equation 3.1 can be used twice to derive the relationship shown in Eq. 3.2 relating the distances from the lenses to an opening, $d_1$for lens 1 and d_2 for lens 2, and the focal lengths of the lenses, f_1 for lens 1 and f_2 for lens 2.

$$\frac{f_2}{f_1} = \frac{d_2}{d_1} \tag{3.2}$$

Equation 3.2 is also used to guide the choice of the size of the pinhole that is used to clean up the beam and ensure that only the light propagating through the core is measured. The pinhole is chosen to be approximately 30% larger than the core. This will decrease the likelihood that the fundamental mode will be clipped at the pinhole, yet still stop the light that propagates in the cladding of the capillary.

In order to quantify the experimental results, a model was written in MATLAB to calculate and plot the transmission through a waveguide. The loss in transmission is

exponential with respect to length; with an attenuation constant of α which is defined in units of loss per length [7],

$$\alpha_{nm} = \left(\frac{u_{nm}}{2\pi}\right)^2 \frac{\lambda^2}{a^3} \frac{\frac{1}{2}(n^2+1)}{\sqrt{n^2-1}} \tag{3.3}$$

where u_{nm} is the propagating mode, n is the index of refraction of the waveguide cladding, a is the radius of the waveguide, and λ is the wavelength of the laser light. Due to the propagating mode being the fundamental mode u_{nm} is equal to 2.405 the first zero crossing of a 1st order Bessel function, the wavelength is λ=532 nm, and n is approximately to 1.5 for glass. The value of the attenuation constant, for a 25 μm diameter hollow-core capillary using this values in Eq. 3.3, is calculated to be α_{11} = 0.041 1/cm.

For uniformly distributed attenuation, the loss in the propagating intensity due to transmission through the waveguide can be modeled as the initial intensity, I_o, multiplied with the exponential of the attenuation constant multiplied by the length of the waveguide, L.

$$I = I_o e^{-\alpha L} \tag{3.4}$$

Figure 3.1 displays the theoretical intensity through a capillary. Note that this graph assumes a theoretical maximum transmission of 80% [7], with low bending and coupling losses.

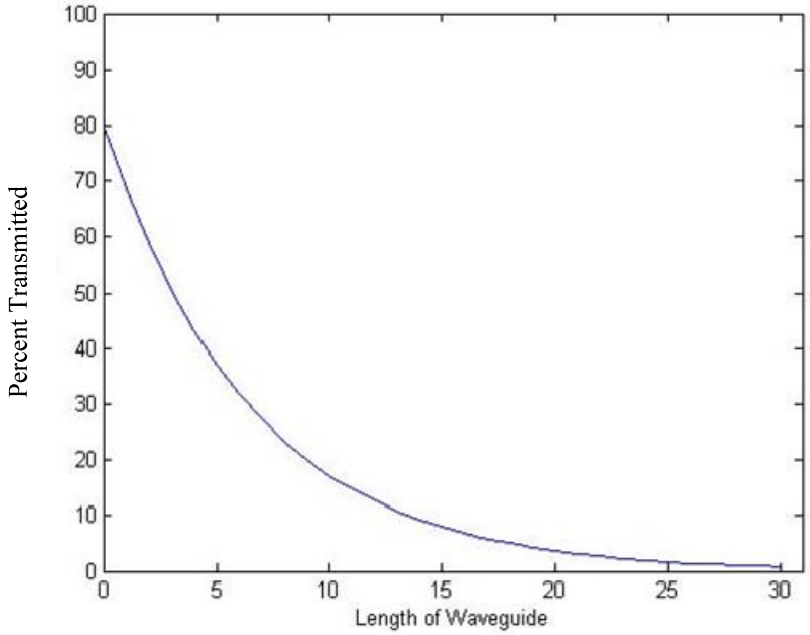

Figure 3.1: Theoretical Transmission vs. Waveguide Length for light propagating through an optical waveguide.

Experimental Setup

The experimental setup consists of the laser beam from the Verdi V-10 laser with wavelength 532 nm, coupled into a single-mode fiber to ensure that the coupling beam into the glass capillary consists of only the fundamental mode. A second fiber coupler is utilized to collimate the laser beam out of the single-mode fiber. Using the ratio of ω/a, the required beam spot size in the 50 μm capillary is calculated to be 32 microns in diameter, and requires a lens that will focus to a spot of the same diameter. Using Equation 3.1, the lens focal length is calculated to be 75.6 mm. The laser beam is then directed into the hollow core of the glass capillary via the 75.6 mm coupling lens. In

order to accurately steer the beam into the core of the capillary, a Z-fold mirror arrangement is used, as depicted in Figure 3.2.

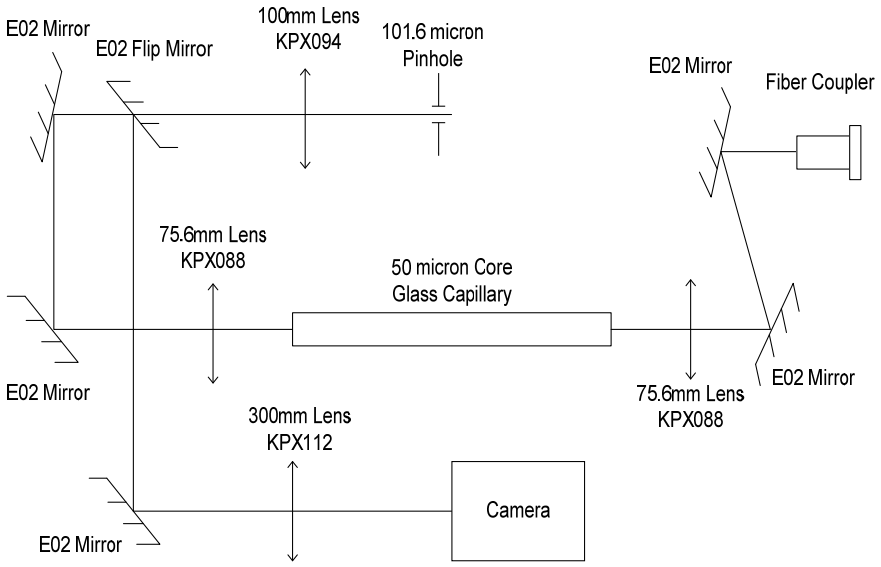

Figure 3.2: Lab Bench Setup to Couple laser light into a Glass Capillary

The glass capillary requires a mounting system that constrains the capillary in XYZ space at the coupling face, holds the output face to minimize the bend in the capillary, and allows for the capillary's length to be decreased while maintaining the coupling position. A rail is utilized to maintain the Y position of the pedestals to prevent the glass capillary from bending horizontally as the rear pedestal is moved closer to the coupling pedestal. The mounting system consists of two pedestal mounts and two custom machined v-blocks, one for each pedestal. The pedestal mounts are shown in Figure 3.3 to allow the reader to better understand the custom mounts.

Figure 3.3: Custom V-Block Mounts on Pedestals

Once the laser beam is passed through the capillary, the beam is collimated using a second 75.6 mm lens. A flip mirror is used to redirect the laser beam through a 300 mm focusing lens and onto a camera. The camera is used to monitor the output from the capillary, allowing for the laser beam to be coupled into the fundamental mode.

Once the laser beam is coupled into the fundamental mode, the flip mirror is flipped down, allowing the laser beam to be directed into a pinhole. The display from the camera is a monitor which has a marker point on it indicating the location of the capillary core. This point allows for the pinhole to be quickly aligned when the capillary is cut down. A second Z-fold is used to make fine adjustments in the beam path to direct the spot into the pinhole and maximize the output, which images the mode exiting the capillary. A 101.6 micron pinhole is used, and the laser beam is focused through it via a 100 mm lens. The use of the pinhole allows for the measurement of the energy that is propagating in the fundamental mode in the capillary while blocking the light that propagates through the glass portion of the hollow core capillary. Once the beam passes

through the pinhole, it is imaged on a target screen. The target screen is used to verify that the mode is passing through the pinhole without clipping prior to taking a power measurement.

Results

A total of four experimental data sets were taken, with a coupling efficiency into the capillary of 11.4%, a 50 μm core diameter capillary, and the dual-pedestal capillary mounting system. The data gathered from the experiments are displayed in Figure 3.4, showing an exponential decay in the amount of transmitted power as the length of the capillary is decreased.

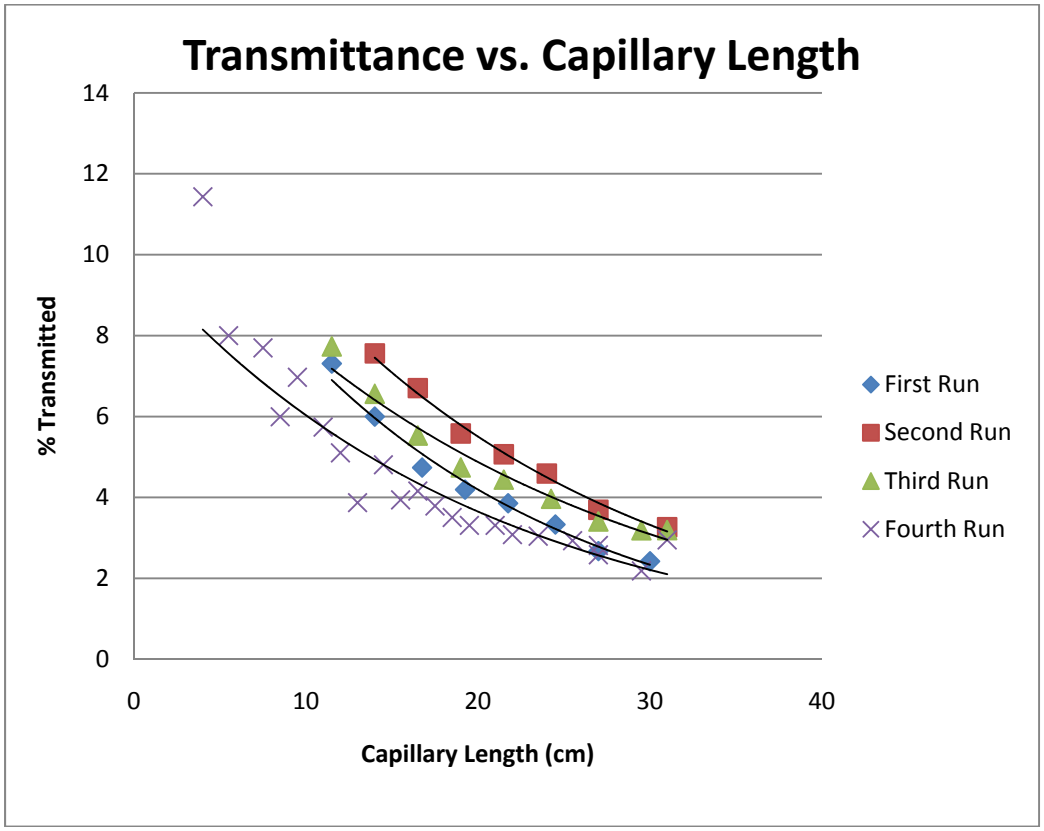

Figure 3.4: Plot of Transmittance vs. Capillary Length

The exponential coefficient and the y-intercept of the exponential fit lines are shown in Table 3.1. Table 3.1 also shows the theoretical loss with a y-intercept of 80%, which is estimated from minimal losses due to bending and coupling [7]. The exponential coefficient average (0.053 loss per cm) is within 22.6% of the full diameter theoretical attenuation constant (0.041 loss per cm, from discussion following Eq. 3.3). The average power due to just coupling loss is fitted to be 12.88% of the incident power. The α term ranges from a loss of 4.6 per meter to a loss of 5.9 per meter over the four series of data, while the transmission percentage immediately after coupling ranges between 10.73 and 15.11%.

Table 3.1: Y-Int (%) and Alpha for Data Sets

	Y-intercept (%)	Exp Coefficent
First Run	13.54	0.059 Loss per cm
Second Run	15.11	0.050 Loss per cm
Third Run	12.13	0.046 Loss per cm
Fourth Run	10.73	0.056 Loss per cm
Average	12.88	0.053 Loss per cm
Theory	80	0.041 Loss per cm

Discussion

While coupling into the capillary, it is important to be coupling into the fundamental mode. This is achieved using two techniques: the first is with a camera linked to a display, while the second involves a negative lens and a target card. Both of these techniques allow for the observation of the mode in the core of the capillary as the incident laser beam is steered into coupling with the fundamental mode.

With the 532-nm laser light that is used, it is possible to observe the fine impurities in the core-to-cladding interface of the capillary. Light scatters out of the capillary at these points, and provides a location as to where the extra losses are occurring in the capillary. These impurities are sources of the excess loss that is experienced, and this knowledge will assist in determining the quality of glass capillaries that will be used in future experiments.

The coupling loss in the glass capillaries immediately after coupling (capillary length ≈ 0 cm) is significant, as it was experimentally measured to be over 85%. Not all of this loss is directly attributed to the coupling loss alone. Other areas that account for loss are in the lenses and mirrors that are used, as neither type of component is perfectly designed to contain absolutely no losses, yet the loss in these areas totals ~4% and does not explain all of the loss. Another area that contributes to the losses is at the pinhole, which is designed to block the light. The losses at the pinhole are theoretically insignificant as the size of the pinhole was chosen to be 30% larger than the beam spot at the location of the pinhole. Even considering all of these areas of loss in the system, there should be a greater amount of light that is propagated through the core. The large coupling loss may be due to the laser beam not perfectly mode matching with the capillary.

The attenuation constants that were experimentally found are within 37% of the theoretical value. This deviation may be due to a combination of two points of inconsistency in the system. These include: 1) the fluctuations of the laser itself, which required all measurements to be taken twice to average out changes in output power from

the laser; 2) the potential for errors in the power meter itself. The power head was observed to have been scored in portions of the active sensing area, which caused the power readings to be diminished if the laser beam became incident in the damaged areas.

Fitting the experimental data yields an exponential curve fit to the data, as shown in Figure 3.4; with the experimental α 20% larger than the theoretical α. A reason for this is the possibility that the coupling face is not perfectly perpendicular with the core. It is not known how this can be resolved, as current cleaving techniques do not provide a perfect perpendicular face and may cause the core to not have a perfectly round face.

A second source of the deviation is in a slight bend in the capillary itself. All precautions were taken in the execution of the measuring process, yet the need for a capillary stand that can support the entire capillary while allowing for the capillary to be cut down provided only one solution, a multi pedestal mounting system. The downside to this system is the opportunity for a slight bend in the capillary that is not noticeable or apparent during the experiment. The slight bend may attribute to the overall losses observed via the addition of bending losses, leading to poor mode matching in the capillary.

Conclusion

The experimental data of the losses through a hollow-core glass capillary match up to within 23% of the theoretical losses once the unknown experimental losses (i.e. coupling loss) are taken into account. The experimental data did produce the exponential decay line shapes that are expected, just to a less than desirable degree. An interesting observation regarding the hollow core glass capillaries is that it is possible to observe the

impurities at the core-cladding interface. The light scatters out of the capillary at the points of impurity, and provides a guide as to the location of large impurities in the capillary that cause extra transmission loss.

CHAPTER 4 – SECOND HARMONIC GENERATION USING A KTP CRYSTAL

Introduction

Second Harmonic Generation (SHG) allows for an output wavelength that is half the length of the incident wavelength via photon conversion. Photon conversion is when two photons of the same wavelength propagate through a medium and exit the medium as one photon of a new wavelength. The usefulness of SHG is that a desired wavelength, which is difficult to produce by conventional stimulated emission, is able to be created with readily available materials. In order for light to undergo SHG, two items are needed: 1) light that is uniquely polarized; 2) a special crystal. The uniquely polarized light passes into the special crystal, which is grown and cleaved in such a way that when the incident beam passes into the crystal, the exiting light becomes phased-matched and efficiently produces a new photon through photon conversion.

Theory

There are two main types of SHG phase matching and both rely on passing the incident laser beam through a birefringent crystal that affects the speed at which the light propagates in the crystal differently for different polarizations. Type I phase matching takes two incident photons with identical polarization, and produces an output photon that has a polarization that is perpendicular to the incident photons. The second method of SHG is Type II phase matching, in which one of the incident photons is polarized along the ordinary crystal axis and the second incident photon is polarized along the

extraordinary crystal axis. This combination produces a photon polarized in the extraordinary-index crystal plane [8].

To accurately calculate the phase matching condition, Δk, the angular frequency of the incident beam, ω, the speed of light, c, along with the index of refraction at ω and 2ω must be known to complete the calculation. When Eq. 4.1 reaches zero, the maximum amount of incident light is being converted and the two incident photons are perfectly phase matched (see section 8.3 in [9]).

$$\Delta k = \frac{2\omega}{c}(n(2\omega) - n(\omega)) \tag{4.1}$$

With the knowledge of the index of refraction at the two wavelengths and the phase matching condition, the intensity of the SHG light can be calculated from Eq. 4.2 [9]

$$I(2\omega) = 2I^2(\omega)\left(\frac{\mu}{\varepsilon}\right)^{3/2}\frac{\omega^2 d^2 L^2}{n^3} sinc^2\left(\frac{\Delta kL}{2}\right), \tag{4.2}$$

where $I(\omega)$ is the initial intensity at the fundamental angular frequency ω, L is the length of the crystal, n is the index of refraction of the crystal, d is the beam diameter, μ is the permeability of the crystal, ε is the permittivity of the crystal, and Δk is the phase matching condition. It should be noted that the second harmonic intensity is dependent upon the crystal properties and increases quadratically as the input intensity increases. Figure 4.1 displays the normalized result of Eq. 4.2 when θ is swept between -10° to 10° and illustrates the sinc^2 function that is expected. At an entrance angle of 0 radians, the maximum intensity occurs and is shown as a value of 1 in Figure 4.1.

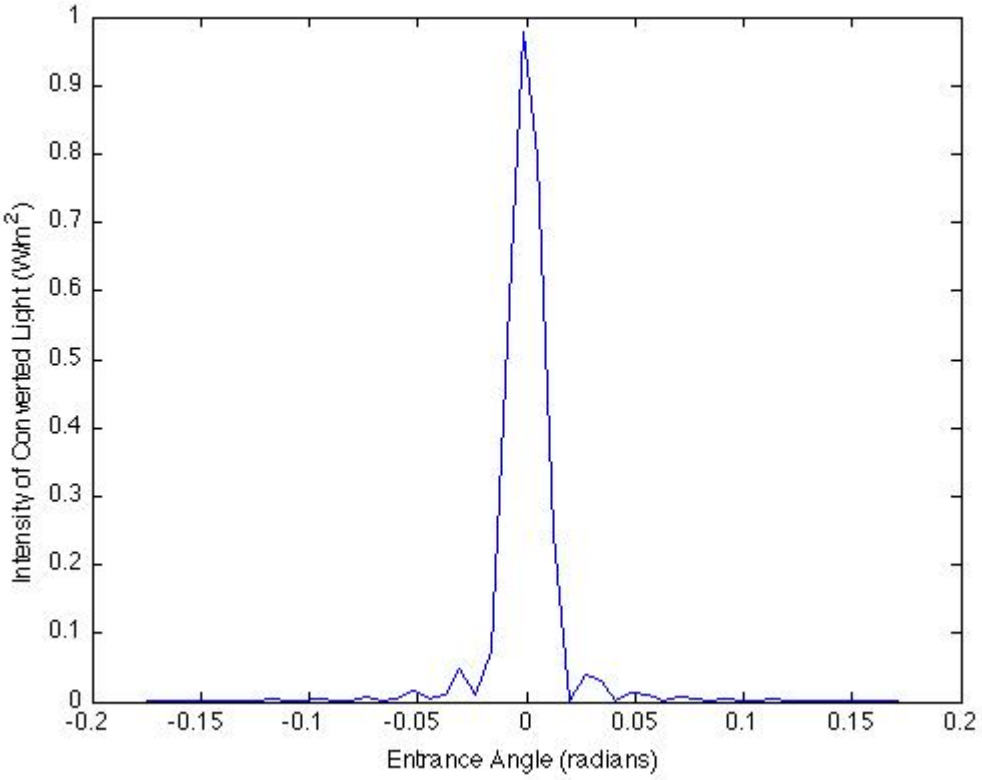

Figure 4.1: Entrance Angle vs. Normalized Intensity

Experimental Setup

The experiment utilizes a continuous wave 1064 nm Nd:YAG laser as the source, which is focused into a single mode fiber via an Optical Fiber Port (OFR) and is collimated using a second OFR. An OFR is a coupler that contains a lens and a fiber connector. The lens either collimates the light exiting an optical fiber which is connected to the fiber connector, or focuses the light into the fiber. Figure 4.2 illustrates the layout of the optical components.

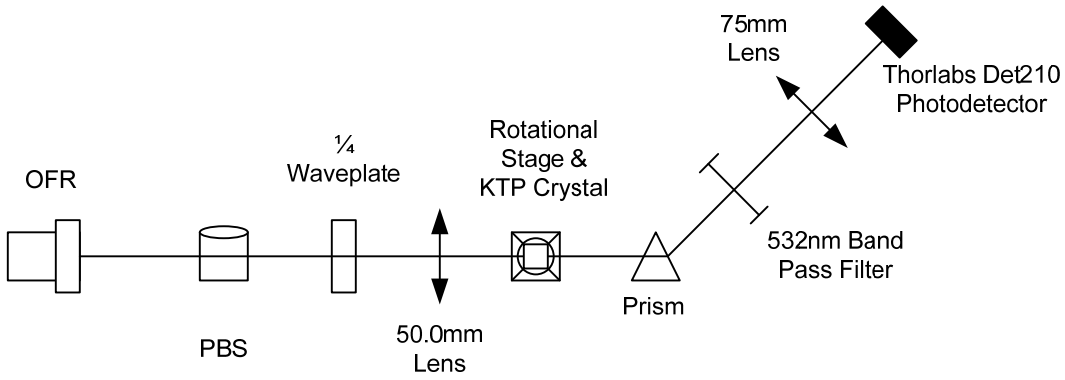

Figure 4.2: Lab Bench Setup for Frequency Doubling

The 1064 nm light is passed through a polarizing beam splitter and a 1064 nm λ/2 plate rotated by 22.5° to ensure that the light is correctly polarized prior to the KTP crystal. The 1064 nm is then focused through a KTP crystal with dimensions of 8 mm x 8 mm x 5.5 mm on a rotational stage via a 50.0 mm lens. The crystal is placed in the center of the rotational stage with the beam passing through the 5.5 mm side of the KTP crystal. Once the beam exits the crystal, the beam passes through a prism which is used to separate the 1064 nm light from the 532 nm light. To further ensure that the only light being measured has a wavelength of 532 nm light, a band pass 532 nm filter is placed in the beam path prior to the photodetector. The 532-nm light is then focused onto a Thorlabs Det210 Photodetector by a 75 mm lens.

Results

The intensity of the 532 nm light was measured as a function of the rotation of the KTP crystal. The crystal was rotated a total of 20°, in increments of 0.5°. When the beam was near perpendicular to the crystal face, the rotation angle was changed to increments of 0.25°, which provided a greater resolution of the measured intensity. The data were normalized and fitted to the function $f(x) = A * sinc(Bx)^2$ with an R^2 value of 0.9893. The closer the R^2 value is to 1, the more accurate the theoretical approximation is to the experimental data. This fit is shown, along with the data points, in Figure 4.3. An entrance angle of zero° corresponds to the crystal face being perpendicular to the laser beam.

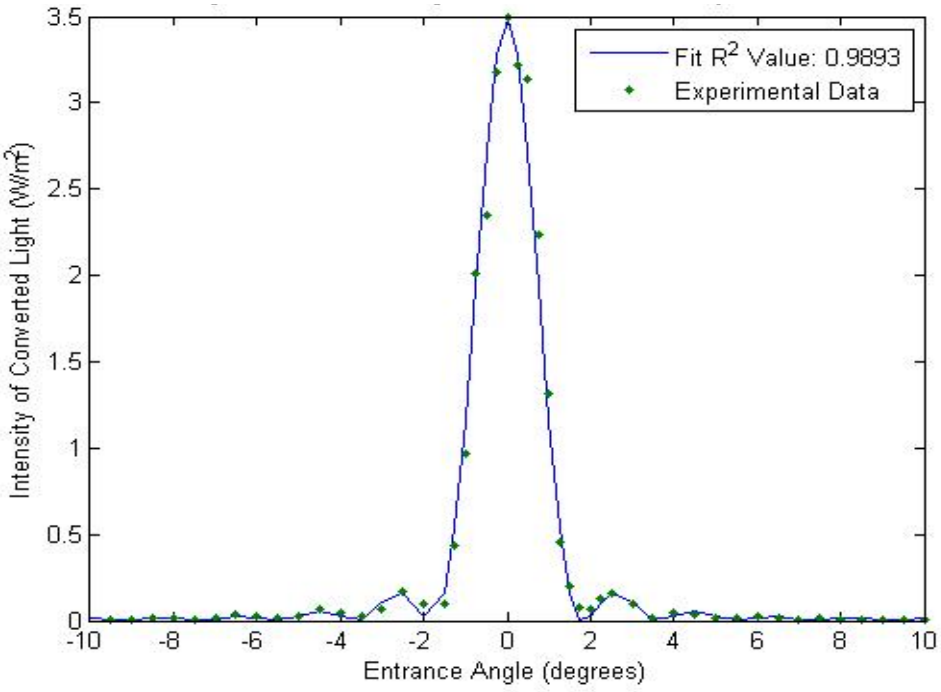

Figure 4.3: Entrance Angle vs. Normalized Intensity with Fit

The initial power from the 1064 nm laser is measured five times and averaged, as shown in Table 4.1. The average is used to calculate the efficiency of the KTP crystal when the maximum amount of light is converted. The maximum converted light, with an input beam power of 183 mW, is recorded to be 11 μW, giving the crystal an efficiency of 0.006%. The SHG light intensity will increase quadratically as the intensity of the input beam increases, resulting in an increase in the conversion efficiency.

Table 4.1: Incident Power from 1064-nm Laser onto KTP Crystal

	Reading 1	Reading 2	Reading 3	Reading 4	Reading 5	Average Reading
Power (mW)	179	178	178	179	180	178.8
Noise in Detector (mW)	.258	.251	.248	.247	.246	.250
Power Without Noise (mW)	178.74	177.75	177.75	178.75	179.75	178.55

Discussion

It is expected from Figure 4.1 that the amount of light converted versus entrance angle into the crystal will follow a sinc^2 fit. The angular acceptance of the KTP crystal from the data sheet is 1.6272°. Angular acceptance, which is also known as acceptance angle and crystal angular tolerance, is defined as the crystal tilt away from the phase matching direction in which $\Delta k*L=2\pi$ [10], which is the first null in a sinc^2 function. The

experimental data has a measured angular acceptance of 1.8329°. The experimental data has an error of 12.6% from the KTP crystal data sheet.

The beam waist is measured utilizing the knife-edge technique. This technique was performed to verify two items: 1) the laser beam is not larger than the crystal, 2) and the crystal is placed in the tightest portion of the beam waist. The position of the knife-edge is recorded at two points, when the laser power is measured to be 84% and 16% of the initial power. At the 84% of initial power point is the leading edge of the beam spot and at 16% of the initial power is the trailing edge of beam spot. The distance between these two points is measured to be 139 microns. Using the Rayleigh range equation solved for the beam waist, $\omega_o = \sqrt{\frac{Z_R \lambda}{\pi}}$ and Z_R is the focal length of the focusing lens. The calculated diffraction limited beam spot size is then 130 microns. The measured beam spot is approximately 7% larger than the calculated size, and is due to the lack of accurately measuring the location of the knife edge and the amount of beam power being measured. The Thorlabs PM100 detector does not allow for accurate measurement at low power levels. The difference in the beam spot measured to calculate represents one of two possibilities; the knife-edge was not positioned at the same point as the KTP crystal face, or the KTP crystal face was not positioned at the exact focal point of the lens.

Conclusion

By utilizing a KTP crystal, it is possible to convert 1064-nm laser light to 532-nm light by the process known as photon conversion. The amount of 532-nm light that is produced by photon conversion in the KTP depends strongly on the incident angle into

the crystal. As the incident angle changes, the intensity of light converted into 532-nm light follows Equation 4.2. The advantage of using the photon conversion technique is quite evident in being able to create a laser beam of a new wavelength that is not reachable by a laser.

CHAPTER 5 – DIFFRACTION GRATING TO SEPARATE THE LASER WAVELENGTHS

Introduction

A diffraction grating consists of a periodic structure of lines, spaced by a distance on the order of the wavelength of incident light on a substrate. Examples of diffraction gratings can be found in CDs, DVDs, and holograms on credit cards. There are two types of diffraction gratings, reflection and transmission. As the incident light interacts with the grating, it is diffracted to a new angle depending upon the wavelength, incident angle of the light, period of the grating, and the diffraction order. This property allows for a diffraction grating to display the wavelength spectrum of the incident light onto an observation plane.

Theory

Due to the properties of the diffraction grating, the Huygens-Fresnel Principle can be implemented. This principle states that every point on the incident wavefront will generate a spherical wave [11]. The strips of material create a path difference between the spherical waves. This path difference induces a phase shift in each of the spherical waves. When the strips of material are at a spacing that provides optical path difference equal to the wavelength, λ, of the incident light, the phase matches up, allowing for constructive interference. The constructive interference will have maxima at specific angles, θ_m . This angle can be calculated using the grating equation [12]

$$\frac{(\sin(\theta_m)-\sin(\theta_i))}{G} = m\lambda \tag{5.1}$$

where G is the number of lines per mm on the grating and λ is the optical wavelength, in this case 1064 nm. The angle of incident θ_i is used with the diffraction order, m, to calculate the precise diffraction angle. Multiple wavelengths are able to be diffracted off the same grating simultaneously from the same angle of incidence. The grating equation is used to calculate the reflected angles for a range of diffraction orders from -3 to 3 1064 nm incident light, which are shown in Table 5.1 for a 600 line per mm grating.

Table 5.1: Calculated Angles off a 600 Lines/mm Grating for 1064 nm

Incident Angle (Degrees)	-3 Order (Degrees)	-2 Order (Degrees)	-1 Order (Degrees)	0th Order (Degrees)	+1 Order (Degrees)	+2 Order (Degrees)	+3 Order (Degrees)
0	-	-	-39.67	0	39.67	-	-
15	-	-	-22.31	15	63.79	-	-
30	-	-50.96	-7.95	30	-	-	-
45	-	-34.72	3.93	45	-	-	-

Experimental Setup

The experimental setup to measure the diffraction grating consists of a 1064 nm continuous wave laser source projecting the collimated beam through free space. The beam is incident onto the desired diffraction grating which is mounted to a rotational stage. The diffraction grating is positioned such that the collimated beam strikes the diffraction grating on the center of the grating.

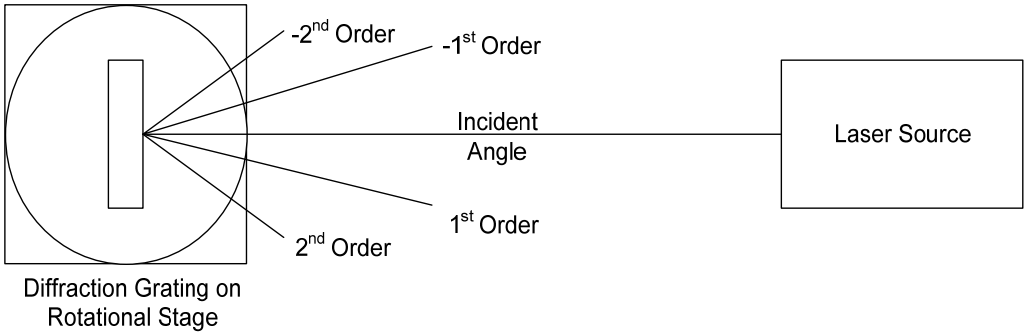

Figure 5.1: Lab Bench Setup for Diffraction Grating Experiment for Incident Angle 0°

An infrared card attached to a target card is used to identify the position of the diffracted beams. Once a diffracted beam is located, a protractor is used to measure the angle between the grating normal and the diffraction order. The grating is then rotated and the angle is measured and recorded. The process is repeated from 0° to 45° angle of incidence in steps of 15°.

Results

The incident light is diffracted off of the grating at various angles dependent upon the incident angle, wavelength, and diffraction order. A negative sign indicates that the diffracted angle is to the left of the diffraction grating normal when observing from above the grating. A positive sign indicates that the diffracted angle is on the same side of the normal as the 0^{th} order. Figure 5.2 displays a graphical representation for the sign

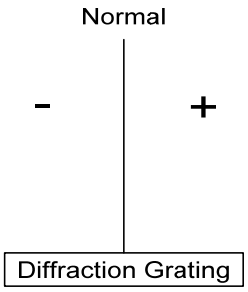

Figure 5.2: Graphical Display of Angle Sign Convention

convention for the diffracted angle. The observed diffraction orders off of the 600 lines per mm grating as the incident angle is increased are shown in Table 5.2. In the table a dash is used to represent angles that are not able to be measured off of the diffraction grating.

Table 5.2: Reflected Angles Measured off Diffraction Grating

Incident Angle (Degrees)	-2 Order (Degrees)	-1 Order (Degrees)	0th Order (Degrees)	+1 Order (Degrees)
0	-	-44	2	45
15	-	24	15	-66
30	-	-7	30	-
45	-47	6	-	-

Discussion

It is noticed immediately that the sign convention between the theoretical diffracted angles and the experimentally found diffracted angles is reversed. This is most likely due to how the sign convention is established. The experimental sign convention

was established from a top down point of view, with a positive sign for all angles to the right of the normal, and a negative sign for all angles to the left of the normal. The theoretical sign convention is established from Eq. 5.1, and a positive sign is used for all angles to that are on the same side of the normal as the 0^{th} order, while a negative sign is used for all angles on the opposite side of the normal as the 0^{th} order.

The measured angle for the light diffracted off of the diffraction grating has an error uncertainty of approximately ±4° due to the nature of the measuring technique. The technique involves using a protractor with an arm and an infrared viewing card. Due to the nature of the infrared viewing card, which fluoresces under near infrared light a larger spot then the actual beam spot, the precise location of the beam center is only approximated. The experimental angles for the location of the diffracted orders are within the estimated measurement error for the -1 and +1 diffraction orders once the sign of the angle is switched to the sign convention of Eq. 5.1. At the higher diffraction order for the higher angle of incident, the -2 order was not measured and measurement error doubled for the angles of incident 30° and 45°, respectively.

Conclusion

It is shown that by utilizing the diffraction grating equation, a set of expected diffraction angles is obtained for a given grating, wavelength, and incident angle. The benefit of a diffraction grating is that the diffraction angle is dependent upon the incident wavelength. This is a benefit in that a diffraction grating can be used to separate the incident light into the separate wavelengths, much like a prism. The advantage over a

prism is that the grating has a smaller footprint (i.e. takes up less space) due to the larger diffraction power. In addition to taking up less space, it is also possible for a diffraction grating to be reflective. This allows for a specific order to be guided through an optical system with fewer components than a prism.

CHAPTER 6 – RAMAN CONVERSION

Background

Raman conversion, also known as Raman scattering, occurs when a photon is scattered off of an atom or molecule inelastically. If the molecule is excited by the passing laser pulse, the molecule either vibrates or rotates and releases a photon. There are two types of Raman scattering, Stokes and anti-Stokes, depending on if the molecule absorbs or releases energy [13]. The wavelength of the released photon is dependent upon the change in energy, and is shown in Figure 6.1.

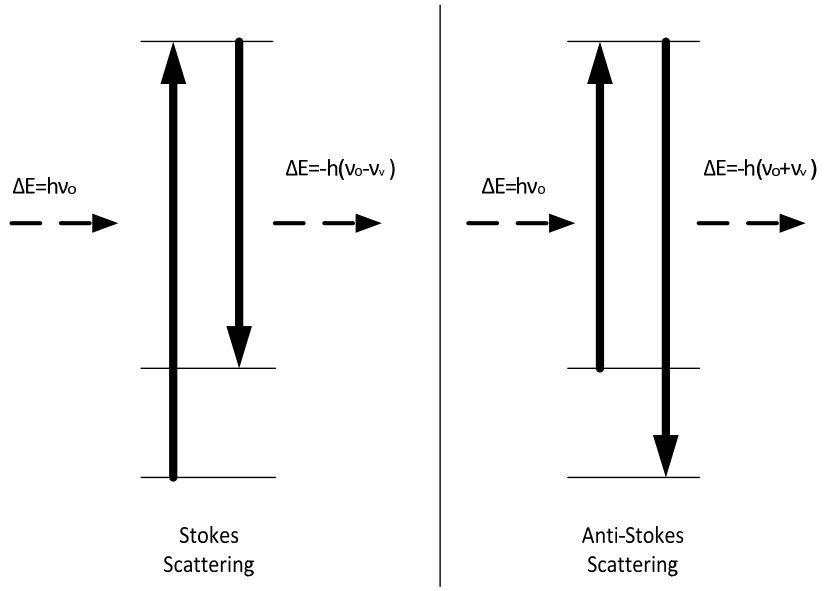

Figure 6.1: Raman Conversion Energy Levels

Results and Discussion

The laser system was observed producing multiple visible and near-infrared wavelengths when the laser pulse is set to 1064 nm and a 100 μm hollow-core capillary. The capillary is filled with Hydrogen gas and pressurized to 100 PSI with the polarization set to excite both the rotational and vibrational Raman energy levels. A visible camera is used to capture the visible Raman conversion wavelengths, and shown in Figure 6.2. From Figure 6.2, it is noted that the 1st through 4th vibrational anti-Stokes conversion wavelengths are observed in two diffraction orders. The first anti-Stokes wavelength is $\lambda = 738$ nm and can be seen as the

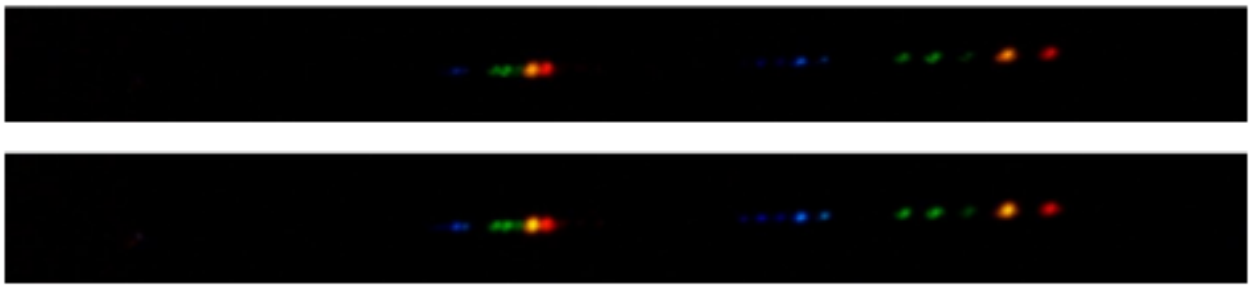

Figure 6.2: Visible Camera anti-Stokes Raman Conversion Wavelengths

deep red spot on the right of the diffraction order. The second anti-Stokes is at $\lambda = 564$ nm, the third anti-Stokes is at $\lambda = 457$ nm, the fourth anti-Stokes is at $\lambda = 384$ nm, and can be seen as a green spot, blue spot, and violet spot in the diffraction order respectively. Figure 6.2 also shows some rotational Raman conversion wavelengths in addition to the vibrational Raman conversion wavelengths. An infrared (IR) camera was used to capture the diffracted light simultaneously with the visible camera, and the

IR image is shown in Figure 6.3 with an arrow to designate the location of the pump 1064 nm light. The 1064 nm spot is of low intensity due to the use of a 1064 nm filter to

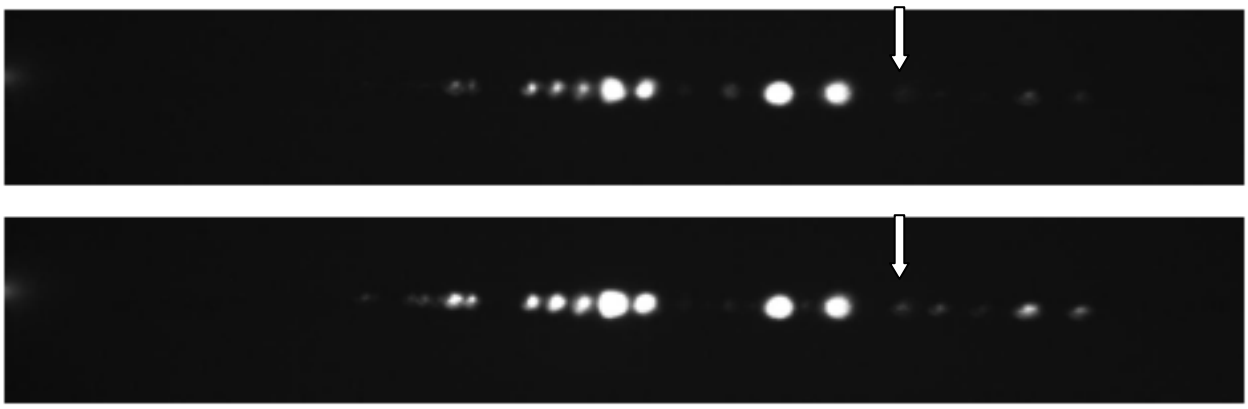

Figure 6.3: Infrared Camera anti-Stokes Raman Conversion Wavelengths

prevent the IR camera from being saturated. Figure 6.3 also shows that near-IR rotational wavelengths from the 1064 nm pump pulse are produced.

The Raman conversion results demonstrate that a 1064 nm beam pulse, when mode matched, is capable of producing visible light down into the violet portion of the light spectrum. Further experiments are needed to measure the amount of power that is produced in each of the anti-stoke wavelengths. The conversion efficiency can then be calculated and compared with the wavelength conversion efficiency of an OPO laser system.

CHAPTER 7 - CONCLUSION

By efficiently coupling into a hollow-core glass capillary, it was experimentally shown that the capillary behaved as a waveguide that was capable of propagating the lowest order mode effectively. This allowed the use of gas as the Raman conversion medium in a confined waveguide and the transmission losses are based largely on the bending of the capillary. The pump wavelength was able to be frequency doubled using a KTP crystal, with the acceptance angle experimentally measured and found to correlate with the theoretical acceptance angle. A diffraction grating was used to separate the Raman converted wavelengths onto an observation screen with the location of the diffraction orders calculated.

The Raman conversion laser system has proven to be a way to not only generate the 1^{st} and 2^{nd}, but also the 1^{st} through 4^{th} anti-stokes wavelengths when a 1064 nm laser pulse is mode matched with the capillary. This means that the light exiting the capillary will be a "rainbow" comprising of the pump wavelength, Stokes wavelength, and anti-Stokes wavelength all propagating in the same direction as shown in Figure 6.2. The rainbow of wavelengths propagating from the end of the capillary causes a problem for any counter measures that an imaging system may attempt to employ. Further developments in the system will optimize the amount of energy that is transferred into the Stokes and anti-Stokes wavelengths, allowing for more energy to bypass the optical filters placed in front of an imaging sensor.

REFERENCES CITED

[1] Personal communication, Dr. Zeb Barber, Montana State University Spectrum Lab (Tel. 406-994-5925).

[2] Schriever, Christian, Stefan Lochbrunner, Patrizia Krok, and Eberhard Riedle. "Tunable Pulses from below 300 to 970 Nm with Durations down to 14 Fs Based on a 2 MHz Ytterbium-doped Fiber Sytem." Optics Letters 33.2 (2008): 192-94.

[3] Peuser, Peter, Willi Platz, Gerhard Ehret, Alexander Meister, Matthias Haag, and Paul Zolichowski. "Compact, Passively Q-switched, All-solid-state Master Oscillator–power Amplifier-optical Parametric Oscillator (MOPA-OPO) System Pumped by a Fiber-coupled Diode Laser Generating High-brightness, Tunable, Ultraviolet Radiation." *Applied Optics* 48.19 (2009): 3839-845.

[4] Barber, Zeb, Christoffer Renner, Randy Reibel, Stephen Wagemann, Randall Babbitt, and Peter Roos. "Conditions for Highly Efficient Anti-Stokes Conversion in Gas-filled Hollow Core Waveguides." Optics Express 18.7 (2010): 7131-137.

[5] Wagemann, S. S. (2009). Building a Raman Laser Pump Source Capable of Generating Flexible Pulse Durations while Maintaining High Spatial Quality. Montana State University. http://etd.lib.montana.edu/etd/2009/wagemann/WagemannS0509.pdf

[6] R. Nubling and J. Harrington, “Launch conditions and mode coupling hi hollow-glass waveguides,” Opt. Eng. 37(9), 2454-2458 (September 1998).

[7] E.A.J. Marcatili and R.A. Schmeltzer, “Hollow metallic and dielectric waveguides for long distance optical transmission and lasers,” The Bell System Technical Journal, 1783-1809 (July 1964).

[8] P.M. Petersen, “Frequency Doubling and Second Order Nonlinear Optics”, Tutorial, DTU Fotonik, http://www.ist-brighter.eu/tuto11/CONF2/Cambridge_Petersen.pdf, last visited 11/6/2011.

[9] Yariv, Amnon. Optical Electronics. 4th ed. Saunders College, 1991. Print.

[10] SNLO Software, “Help File”, http://www.as-photonics.com/SNLO.html, last visited 11/6/2011.

[11] B.E.A. Saleh and M.C. Teich, “Fundamentals of Photonics”, 2nd ED.

[12] Newport, “Diffraction Grating Handbook” 6th Ed.

[13] F. Benabid, G. Bouwmans, J. C. Knight and P.St. J. Russell, “Ultrahigh Energy Laser Wavelength Conversion in a Gas-Filled Hollow Core Photonics Crystal Fiber by Pure Stimulated Rotational Raman Scattering in Molecular Hydrogen” PRL 93 (2004) 123903